Materials Today Physics 15 (2020) 100252

Contents lists available at ScienceDirect

Materials Today Physics

journal homepage: https://www.journals.elsevier.com/materials-today-physics

Alloy amorphization through nanoscale shear localization at Al-Fe interface

F.C. Liu [a], P. Dong [a, b, *], J. Zhang [b], W. Lu [b, c], A. Taub [c, b], K. Sun [c]

[a] Department of Naval Architecture and Marine Engineering, University of Michigan, Ann Arbor, MI, 48109, USA
[b] Department of Mechanical Engineering, University of Michigan, Ann Arbor, MI, 48109, USA
[c] Department of Materials Science and Engineering, University of Michigan, Ann Arbor, MI, 48109, USA

ARTICLE INFO

Article history:
Received 16 May 2020
Received in revised form
17 June 2020
Accepted 30 June 2020
Available online 4 July 2020

Keywords:
Amorphization
Nanoscale shear localization
Interfacial premelting
Dissimilar materials interface
Intermetallic compounds
Interfacial microstructure

ABSTRACT

Achieving reliable metallic bonding directly between steel and aluminum alloys has a broad societal impact on sustainability from transportation systems to space exploration and biomedical devices. This is because steel and aluminum alloys are the top two most available and widely used metals. However, the development of detrimental intermetallic compounds (IMCs) at the Al-Fe interface has frustrated researchers and engineers for decades. Here, we present a new mechanism on how a nanoscale amorphous layer can be introduced at the Al-Fe interface without undesirable IMC: (i) a rapid sliding at the Al-Fe interface can generate a nanoscale premelting layer, leading to nanoscale shear localization; (ii) the resulting high shear strain rate within the premelting layer is high enough to suppress crystallization; (iii) as long as sufficiently high shear strain rate can be sustained within the premelting layer until the interfacial temperature is low enough, a stable amorphous can be retained without relying on rapid solidification. The findings provide a mechanistic basis for devising novel alloy amorphization and dissimilar metal joining techniques.

Introduction

Achieving optimum product functionality and structural lightweighting requires joining solutions for multimaterial components, which broadly benefits human society from infrastructure to space exploration and vehicles [1]. Unfortunately, undesirable thick (often brittle) intermetallic phases and associated cracking developed at bimetallic interfaces, particularly between steels joined with aluminum, titanium, and copper alloys have been the major issues for decades. Among the various material combinations, the Al−Fe bimetallic system is of great scientific and engineering interest as steels and aluminum alloys are the top two most widely used metals.

It has been well established that the formation of detrimental intermetallic compounds (IMCs) at the Al-Fe interface is the major barrier for adopting Al-Fe bimetallic structures assembled through either fusion or solid-state joining process as load-bearing members in safety-critical structures [2,3]. Conventional approaches for mitigating these IMCs have been focusing on metallurgical means of influencing diffusion and phase transformation kinetics by reducing peak joining temperature and/or dwell duration at high temperature [4,5]. These efforts only resulted in limited improvement in reducing the size or amount of interfacial IMC involved, while the problem of preventing IMC formation remains unsolved to a large extent.

The occasional occurrences of a nanoscale amorphous phase at the Al-Fe joint interface under certain conditions that are not well understood have been reported [6]. Such a nanoscale amorphous interface has been credited to higher bond line strengths than those specimens with interfacial IMC [6]. However, without a clear understanding of the amorphous phase formation mechanisms, it is difficult to replicate and control the development of interfacial amorphization for engineering applications. Three hypotheses on the potential mechanisms involved were proposed as follows: (i) rapid solidification with a cooling rate beyond 10^7 K/s experienced by a liquid aluminum layer at the interface [7]; (ii) lattice collapse under extremely high stress caused by high-speed impact [8−10]; and (iii) mechanical alloying at the interface [6,11,12]. All three mechanisms are plausible only under high-speed impact conditions such as those involved in explosive bonding processes. However,

* Corresponding author.
E-mail address: dongp@umich.edu (P. Dong).

https://doi.org/10.1016/j.mtphys.2020.100252
2542-5293/

detailed scientific evidence is lacking for substantiating these hypotheses to the extent that a controlled experiment can be conducted to replicate the interface amorphization phenomena. Perhaps for this reason, the occasional occurrences of nanoscale amorphization have been largely treated as a rare metallurgical phenomenon encountered under the certain conditions postulated above.

Our study showed that nanoscale shear localization can be triggered at the Al-Fe interface. The resultant local shear strain rate was high enough to prohibit crystallization and promote the formation of a nanoscale amorphous alloy. The results pinpoint a new mechanism of generating nanoscale amorphous phases at the Al-Fe interface, which is fundamentally different from the available postulations. Knowledge of this mechanism offers the potential for forming new amorphous alloys and the development of novel manufacturing methods for bimetallic structure [13].

Computational and experimental details

Molecular dynamicsimulation method

LAMMPS Molecular Dynamics (MD) Simulator was used for performing all MD simulations reported in this article. The size and orientation of the three-dimensional atomic boxes of the bcc Fe and the fcc Al are illustrated in Fig. 1. Periodic boundary conditions are applied in the x and y directions. Two slabs of atoms, each having 2 nm in thickness, are placed on the outer surfaces of the blocks in the y direction. The atomic slabs serve as reservoirs. The atoms within each reservoir are identical to the adjacent atomic box but no relative atomic movement is allowed within the reservoir (e.g. the atoms in the slab can only move together in rigid body motion). The slab is used to apply a shear to the system. The distance between the two facing surfaces of the Al and Fe blocks is 2 nm, hence

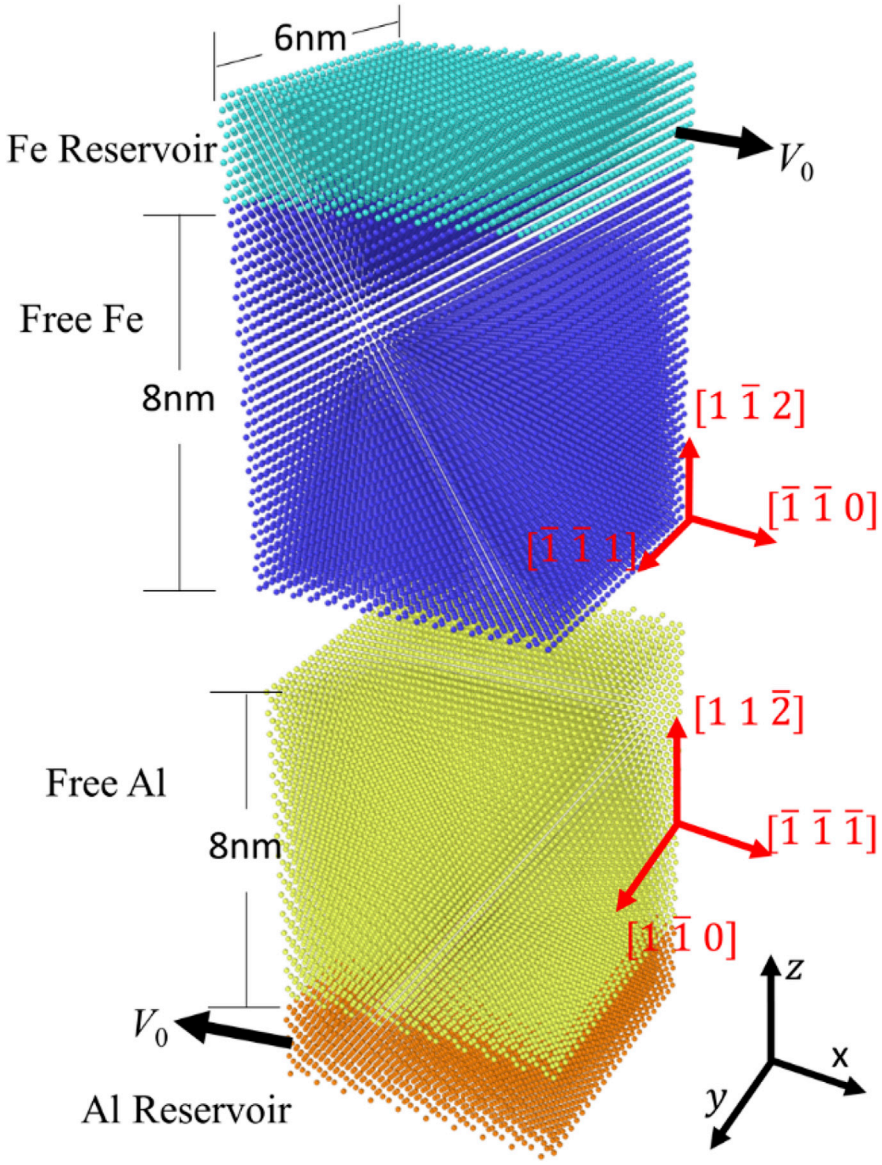

Fig. 1. Atomic structures of the simulation cell.

the interatomic force between Al and Fe atoms is negligible. In this case, the two facing surfaces can be treated as free surfaces. The embedded atom method interatomic potential and NVT ensemble (i.e. the number of atoms (N), the volume (V) and the temperature (T) are conserved) were used for all simulations. The simulation time step was set at 1 fs. To determine the Al surface premelting temperature, the system was increased to various temperatures at a rate of 40 K/ps. The premelting temperature of the Al surface was determined at 890 K. Then two scenarios were simulated. In scenario 1, the Al and Fe blocks were maintained at 890 K for 150 ps and then compressed together to an initial pressure of about 600 MPa by moving the two reservoirs. After this compression step, the distance of the two reservoirs maintained constant in subsequent simulations. In scenario 2, a relative sliding velocity of 0.5 m/s was applied on the two reservoirs after the compression step in scenario 1, and the distance of the two reservoirs maintained constant in subsequent simulations.

To better understand the effect of sliding on the state of atoms at the interface, simulations were also performed starting from 0 K with the Fe and Al atomic boxes compressed together and a sliding velocity of 0.5 m/s applied to the reservoir at the beginning of the simulation. A linear temperature increase of 2 K/ps was applied in the simulation to get more insight into the interfacial premelting phenomena.

Additional MD simulations were conducted to understand the effect of temperature reduction on phase transformation at the Al-Fe interface. After a steady-state liquid was formed at the Al-Fe interface at 890 K and a sliding velocity of 0.5 m/s, the system temperature was reduced to 850 K and the sliding velocity was reduced to 0.3 m/s. For comparison, another simulation was performed with reducing the system temperature reduced to 850 K and stopping the relative sliding after a steady-state liquid was formed at the Al-Fe interface at 890 K.

Interfacial friction experiment

A specifically designed friction stir experiment, as illustrated in Fig. 2, was used to prepare the aluminum-steel interface for investigation. The 6.35-mm thick 6,061 aluminum alloy sheet was placed on the top of an ASTM A36 steel sheet. The faying surfaces were brushed to remove the oxidation before welding. The friction stir tool made of H13 steel had a tapered probe 5 mm in tip diameter and 6 mm in length. During the experiment, the probe rotation speed was set to be 1,000 rpm so that the linear velocity at the edge of the probe tip is close to 0.5 m/s. The travel speed was in the rage of 300–600 mm/min for different samples. The distance between the probe tip and steel surface δ was determined through an analysis of the welded samples after welding. As indicated in Fig. 2, the actual probe plunge depth (x) can be determined with respect to actual weld face width (marked as y). The resulting δ can then be determined. The distance δ involved in this study was in the range of 0.05–0.15 mm.

Microstructure characterization

Samples for cross-sectional examinations were cutoff by water jet from the weld sample and then were ground and polished with standard metallographic techniques. Thin foils about 50 nm in thickness were extracted from the joint interface using a focused ion beam (FEI Helios Nanolab 650) and were analyzed with a JEOL 3100R05 double aberration corrected analytical TEM operated in the STEM mode at a voltage of 300 kV which gives a point-to-point resolution of 0.05 nm.

A post containing the Al-Fe joining interface was extracted from the joint interface using the focused ion beam (FIB) within the vacuum chamber of the FEI Helios Nanolab 650. The post was milled further through FIB annular milling to sharpen the tip containing the Al-Fe interface. The tip radius was shaped to less than 40 nm. Atom probe tomography (APT) analysis was performed using a Cameca LEAP 5,000HR in voltage mode at a specimen temperature of ~55 K. The pulse fraction and the pulse rate were 15% and 200 kHz, respectively. Data analyses were performed using the CAMECA's integrated visualization and analysis software (IVAS).

Surface premelting and interface amorphization

MD simulations were performed to examine the details of surface/interface premelting and its interaction with interfacial shear strain rate in contributing to amorphization development at the Al-Fe interface. At the beginning of the MD simulation, both Al and Fe atomic blocks, separated 2 nm away from each other for negligible interatomic force between the two free surfaces, were heated to various holding temperatures at a constant rate of 40 K/ps. Upon reaching 890 K, a quasi-liquid layer was observed on the free surface of the Al block (Fig. 3a and b), indicating the occurrence of surface premelting below the aluminum bulk melting point (933 K). Similar surface premelting phenomena have been observed on surfaces of metallic crystals and ice at temperatures tens of degrees below material bulk melting point [14–16], which can be attributed to the fact that surface atoms are more weakly bonded than those in the bulk. The resultant premelting layer has lower surface free energy relative to the ordered solid-vapor interface [17].

Two scenarios were then simulated after the occurrence of surface premelting. The first one was to compress the Al and Fe

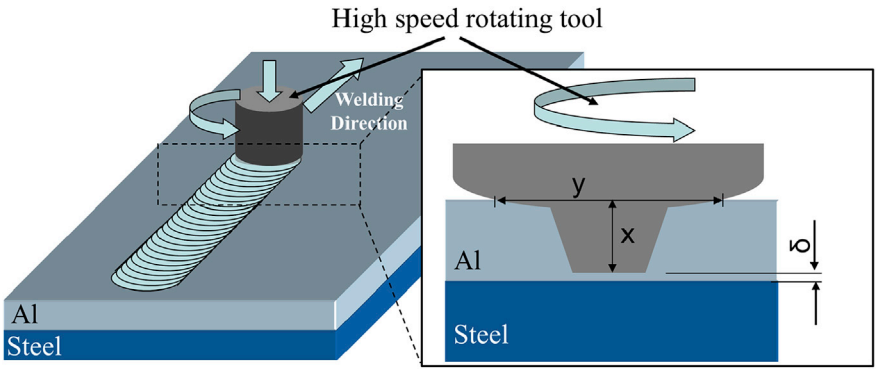

Fig. 2. Schematic illustration of friction stir experiment setup and a cross-sectional view of the friction stir tool position relating to the Al-Fe interface.

blocks together without introducing interfacial sliding between them. The quasi-liquid layer crystallized quickly (Fig.s 3c and d) because the freedom of the Al atoms on the original free surface was significantly reduced upon interfacial bonding. In the second case, a sliding velocity of 0.5 m/s was applied and maintained after the Al and Fe blocks were compressed together. The thickness of the quasi-liquid layer was not only retained but also enhanced (Fig. 3e and f).

To better understand the above phenomena, the atom displacement in the second scenario was further examined after a steady-state of the nanoscale quasi-liquid layer was achieved at the Al-Fe interface. The displacements of atoms within a duration of three ps are presented in Fig. 4a. The atomic displacements within the quasi-liquid layer appear to exhibit a state of disorder. In the adjacent Al and Fe crystals, no relative atom movements can be observed, indicating that the shear deformation was confined within the quasi-liquid layer, that is, nanoscale shear localization occurred at the interface. To further illustrate the details, the atoms were equally partitioned into thin layers (1 Å thick) parallel to the Al-Fe interface. The average atomic displacement in the shear direction is plotted for each layer (Fig. 4b). The atoms within the quasi-liquid layer followed a clear trend: each layer of atoms equally shared the applied shear strain in the shear direction, that is, the resulting shear strain rate distributes homogeneously within the quasi-liquid layer. Therefore, the shear strain rate of each layer of the atoms is equal to the average shear strain rate, as expected for a thin layer of liquid under shear.

The average shear strain rate, by definition, is the ratio of shear velocity and the thickness of the shear zone. As the thickness of the shear zone (quasi-liquid layer) is only 2–3 nm and the applied shear velocity is 0.5 m/s, the resulting shear strain rate within the quasi-liquid layer is higher than 10^8 s^{-1}. Under such an extremely high shear strain rate, the known plastic deformation mechanisms such as dislocation movement and even the faster twinning displacement are not fast enough to accommodate the deformation [18]. The implication is that there is no time for the atoms within the quasi-liquid layer to organize themselves into ordered crystalline structures. A recent investigation has postulated that

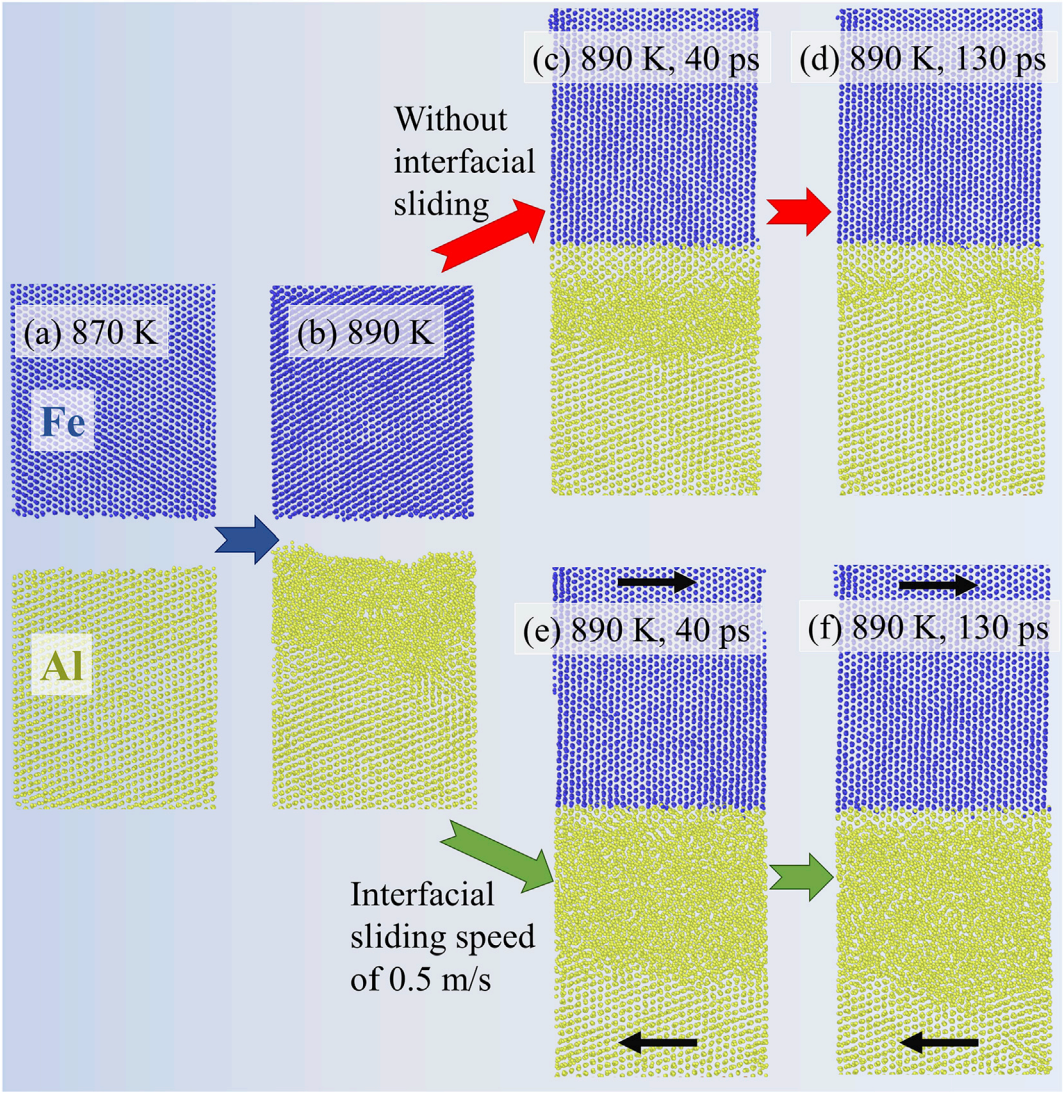

Fig. 3. Snapshots of atom distribution at the Al surface and Al-Fe interface. (a) No evidence of surface premelting when the system was heated to 870 K; (b) Premelting occurred on Al surface at 890 K which was 43 K lower than the melting point of bulk Al; (c) and (d) The quasi-liquid layer crystallized quickly after bonding; (e) and (f) The quasi-liquid layer was maintained at the Al-Fe interface by the applied sliding at a speed of 0.5 m/s.

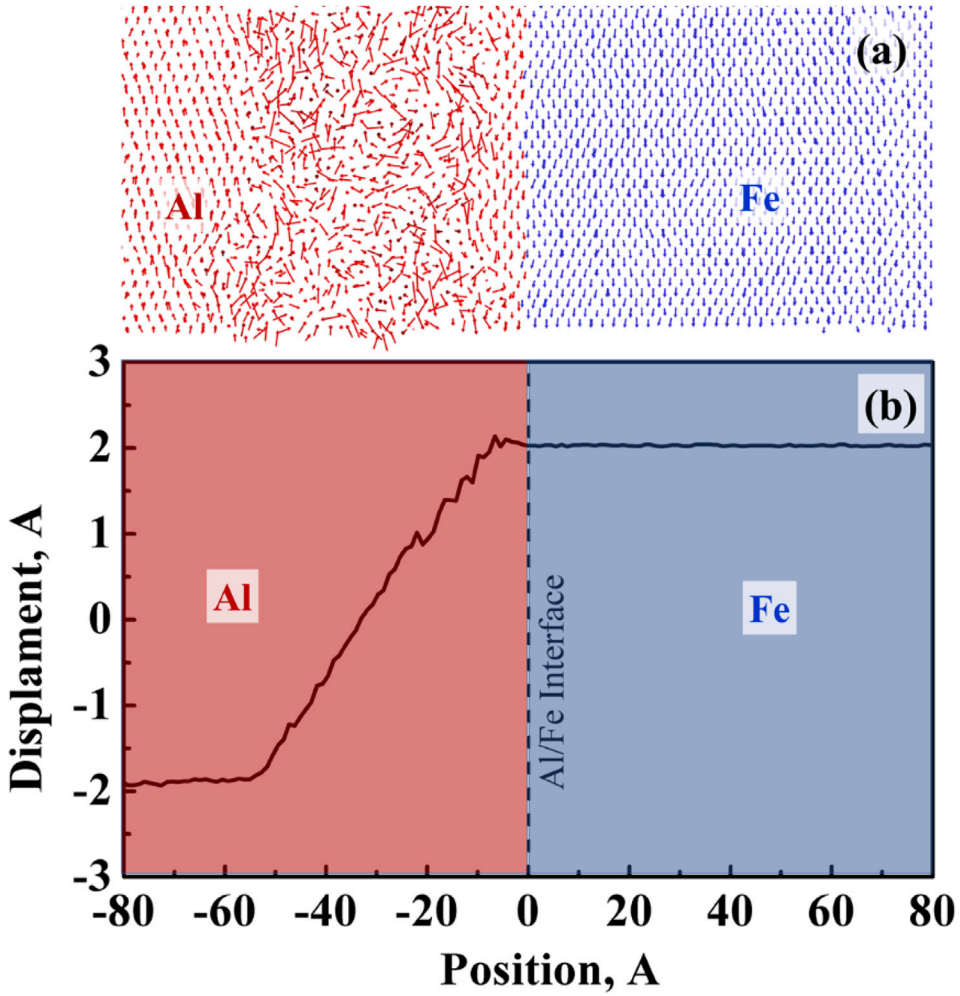

Fig. 4. Atom displacement of Al and Fe atoms during a period of 3 ps when a steady quasi-liquid layer formed at Al-Fe interface under an applied sliding speed of 0.5 m/s: (a) individual atom displacement; (b) average atom displacement within each layer along the shear direction.

deformation mechanisms in crystalline materials can transition from a diffusion process to dislocation movement to twinning, and to the onset of localized shock-induced amorphization as strain rate increases [9], but without providing a plausible triggering mechanism, for example, a premelting state achievable at the nanoscale, as described above.

The results aforementioned show that shear localization along the Al-Fe interface can be introduced by surface premelting at the nanoscale. In most of the friction-based joining or surface processing conditions, a free surface can only be discontinuously created at some points of the interface. A direct contact sliding between aluminum and steel will be the dominant interfacial deformation behavior, for example, the Al-Fe interface studied here. Such deformation conditions were also simulated by MD models (Fig. 5) showing that sliding between the Al and Fe blocks could also generate a premelting layer at the Al-Fe interface when the interfacial temperature reaches $\geq$890 K.

Crystallization suppressed by high shear strain rate

In a practical friction-based bimetal joining application, the ceasing of the interfacial sliding (or shear velocity) results in temperature reduction within the quasi-liquid layer. How would these Al atoms within the quasi-liquid layer respond to a termination of shear actions? To answer this question, two additional MD simulations were performed.

After a steady quasi-liquid layer was formed at 890 K (premelting temperature) at the Al-Fe interface with a sliding velocity of 0.5 m/s, the system temperature was then reduced to 850 K while the sliding velocity was reduced to 0.3 m/s. Under such a condition, a quasi-liquid layer still maintained at the Al-Fe interface (Fig. 6a) even though its thickness was reduced in comparison with that at 890 K and 0.5 m/s. In contrast, the quasi-liquid layer essentially disappeared completely when the system temperature was reduced to 850 K and the sliding velocity was reduced to zero (Fig. 6b). These simulation results show that a sufficiently high shear strain rate is essential in the quasi-liquid zone for delaying or eliminating the crystallization process during solidification.

The fundamental relation between the diffusion coefficient, D, and jump frequency of atoms, Γ, is expressed in the form of $D = \lambda^2 \Gamma/6$, where λ is the jump distance of the diffusing atom. At 890 K, the interdiffusion coefficient of Fe into Al is about 6×10^{-14} m^2/s [19,20]. With the jump distance on the order of atomic spacing of Al or 4 Å, it is estimated that Γ is 2×10^6 s^{-1}. The shear strain rate of 10^8 s^{-1} is much larger than Γ, indicating that two adjacent atomic layers are able to move relative to each other by several lattice spacing before an atomic jump occurs. Thus, the high shear

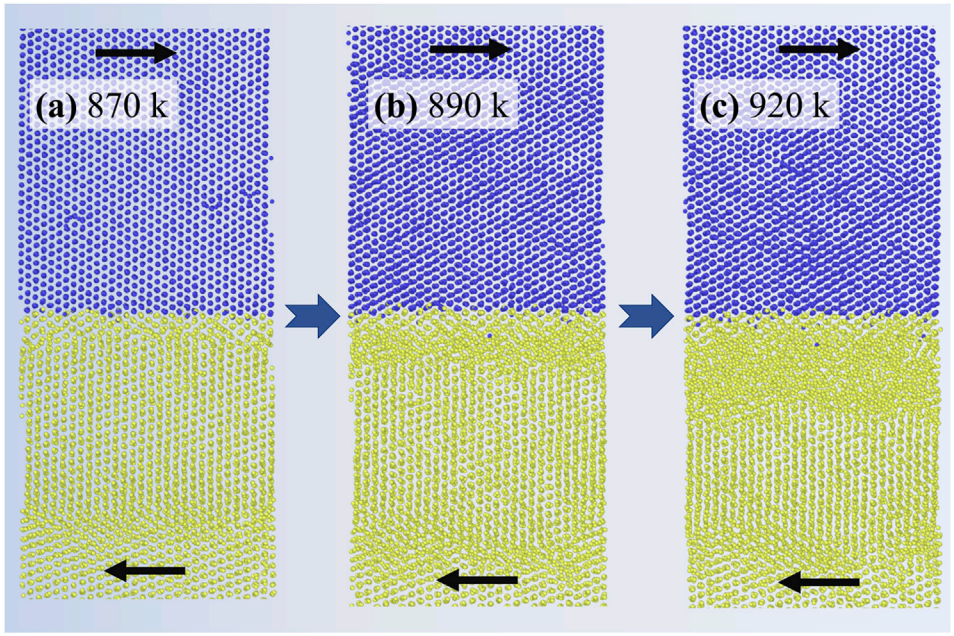

Fig. 5. Snapshot of atomic distribution affected by a sliding velocity of 0.5 m/s at various temperatures: (a) 870 K, (b) 890 K, and (c) 920 K.

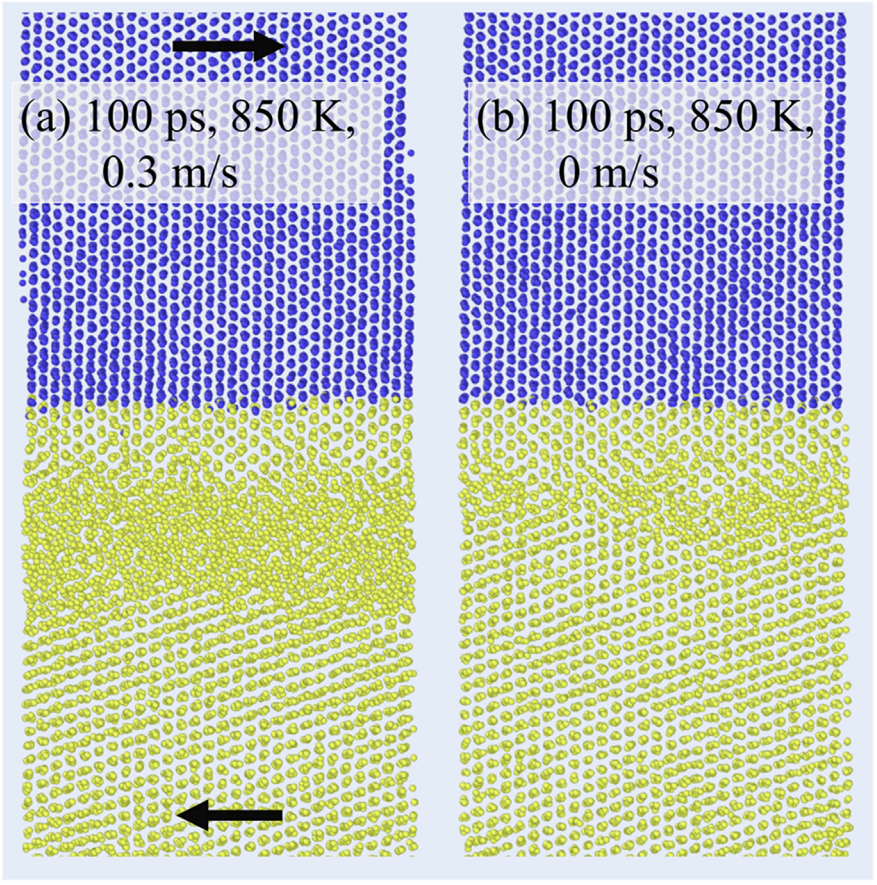

Fig. 6. After a steady quasi-liquid layer was formed at the Al-Fe interface at 890 K and 0.5 m/s, the system was quenched to a temperature of 850 K. Snapshots of atom distribution at the time of 100 ps after the quenching under the conditions of (a) maintaining a sliding speed of 0.3 m/s and (b) no sliding.

strain rate is able to effectively hinder diffusion and suppress the crystallization process.

Experimental verification

Motivated by the MD simulation results, we designed a series of controlled friction stir experiments by creating direct sliding between aluminum alloys and steel so that similar relative shear at the Al-Fe interface can be replicated (Fig. 2). Note that rather consistent joint interface microstructure characteristics were obtained for joints produced at 1,000 rpm and 300–600 mm/min. The details of the interfacial microstructure of the sample produced at 1,000 rpm and 600 mm/min were presented in the following context.

High-resolution transmission electron microscopy (HRTEM) was used to characterize the microstructure at the Al-Fe interface. The boundary of Al alloy and steel in the atomic-scale was identified through HRTEM observations along the [011] direction of the Al alloy and the [011] direction of steel, respectively (Fig. 7). The crystal structure of the Al alloy and steel were confirmed by the arrangement of atoms and the corresponding fast Fourier transform (FFT) patterns. Between the Al alloy and steel, a metallic amorphous layer of 5–20 nm in size can be found, depending on the observed location. The lack of long-range order within the

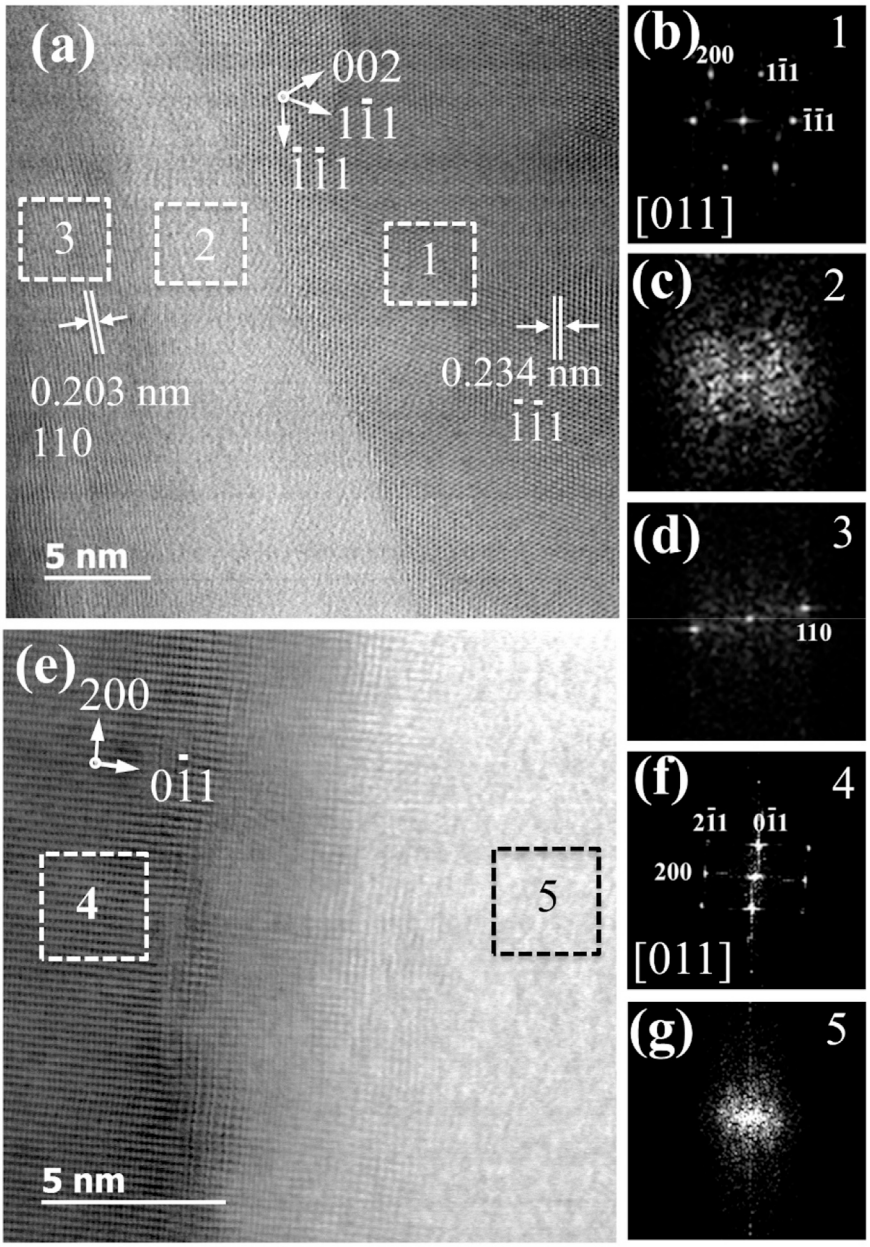

Fig. 7. Microstructure characterization at the Al-Fe interface. (a) HRSTEM image observed along the Al [011] direction. (b) FFT patterns taken from region 1 showing reciprocal fcc crystal structure of aluminum. (c) FFT patterns of region 2 showing a typical feature of an amorphous phase. (d) FFT patterns of region 3 showing feature of reciprocal bcc Fe {110} plans. (e) High-resolution HRSTEM image observed along the Fe [011] direction showing the interface between Fe lattice and the amorphous layer. (f) FFT patterns taken from region 4 showing reciprocal bcc crystal structure of Fe. (g) FFT patterns extracted from region 5 confirming the amorphous phase. FFT, fast Fourier transform.

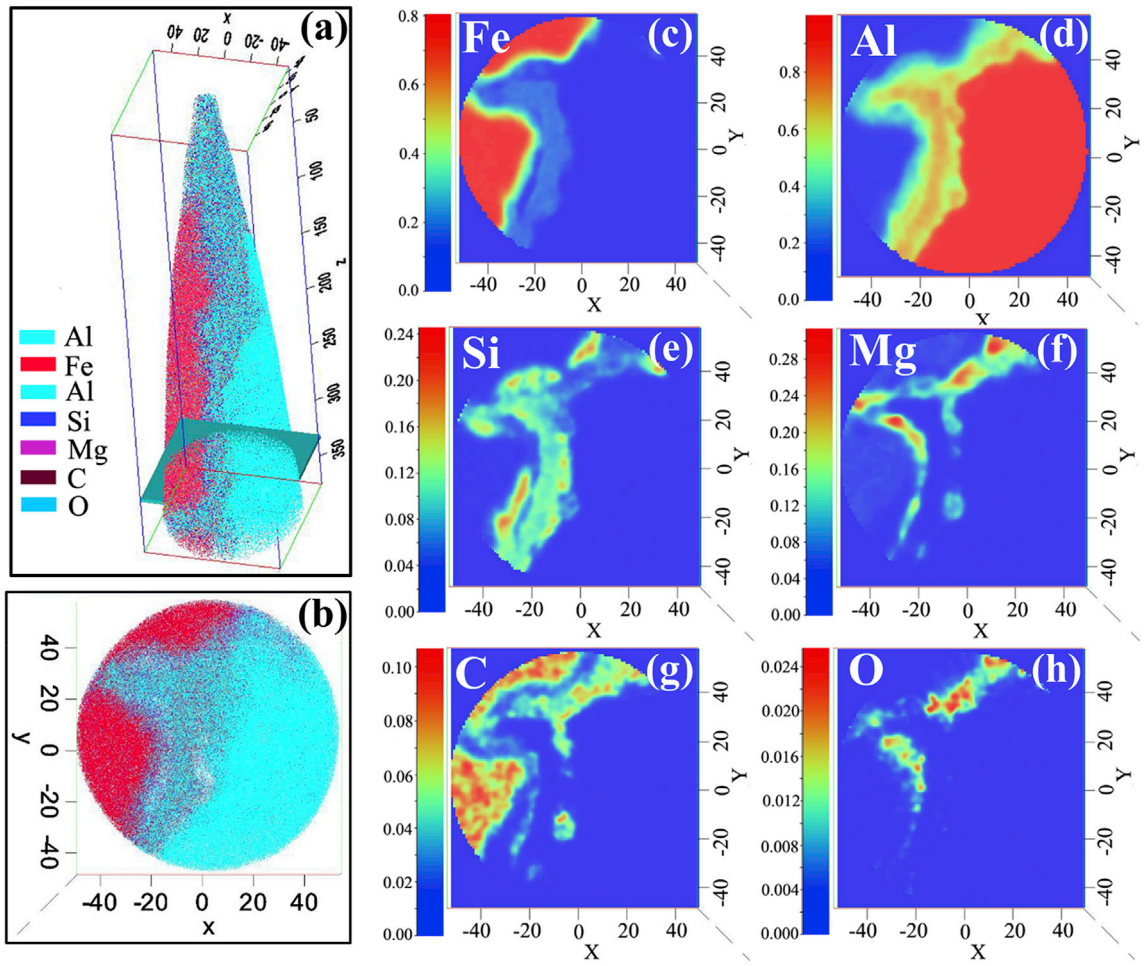

Fig. 8. Atom distributions across the Al-Fe interface analyzed by atom probe tomography. (a) 3D atom distribution and the location of a 2 nm thick data slice. (b) 2D atom distribution within the data slices. (c) to (h) Quantitative atomic concentration within the slices for the element of Fe, Al, Si, Mg, C, and O. 3D, three-dimensional; 2D, two-dimensional.

amorphous layer was confirmed by the corresponding FFT pattern of a diffuse halo which is a typical feature of an amorphous phase (Fig. 7c, and f).

APT which is capable of measuring 3D chemical composition at the atomic scale was used to identify the chemical composition across the Al-Fe interface. The 3D atom map clearly shows a state of atomic mixing at the Al-Fe interface (Fig. 8a). The projection views of a 2-nm thick data slice extracted from the atom probe are presented in the format of an all-element map (Fig. 8b) and individual element maps (Fig. 8c–h), respectively. The individual element maps demonstrate that the atomic mixing zone (amorphous zone in Fig. 7) contains a much higher concentration of Mg, Si, and O than the surrounding Al and Fe crystals (Fig. 8c–h), which is likely formed through a diffusion process from nearby base alloys.

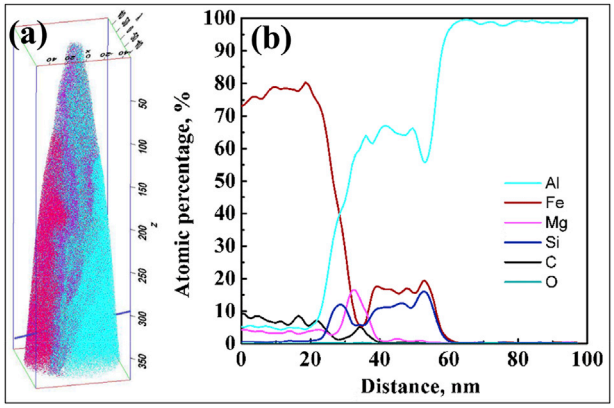

Fig. 9. Atomic distribution within a 1D cylinder across the interface. (a) Position of the cylinder relative to the Al-Fe interface. (b) The atomic distribution within the cylinder 2 nm in diameter was plotted as 1D compositional profiles along the cylinder axis. 1D, one-dimensional.

To quantitively examine the chemical composition across the Al-Fe interface, the concentration of individual elements along the length direction of a 2-nm diameter cylinder was plotted in Fig. 9. The results showed that the major elements within the amorphous region are aluminum. The average chemical composition within the amorphous zone turns out to be close to Al-13.0 at%Fe-17.4 at%Si, a known Al-based glass-forming alloy [21] which would require a critical cooling rate at or beyond 10^6 K s^{-1} for retaining its amorphous state if conventional rapid solidification is used. The cooling rate in our experiments is only about 40 K s^{-1} [22]. Therefore, the metallic amorphous state produced in this study cannot be ascribed to the rapid solidification process defined in a study by Dong and Brust [23]. It is worth emphasizing that the composition of the amorphous region is not simply an average of the elements of the two base alloys. It appears that under the conditions studied, the easy glass-forming composition is preferred. This seems to suggest that increasing the concentration of silicon elements in the aluminum alloys may facilitate the formation of amorphous phase

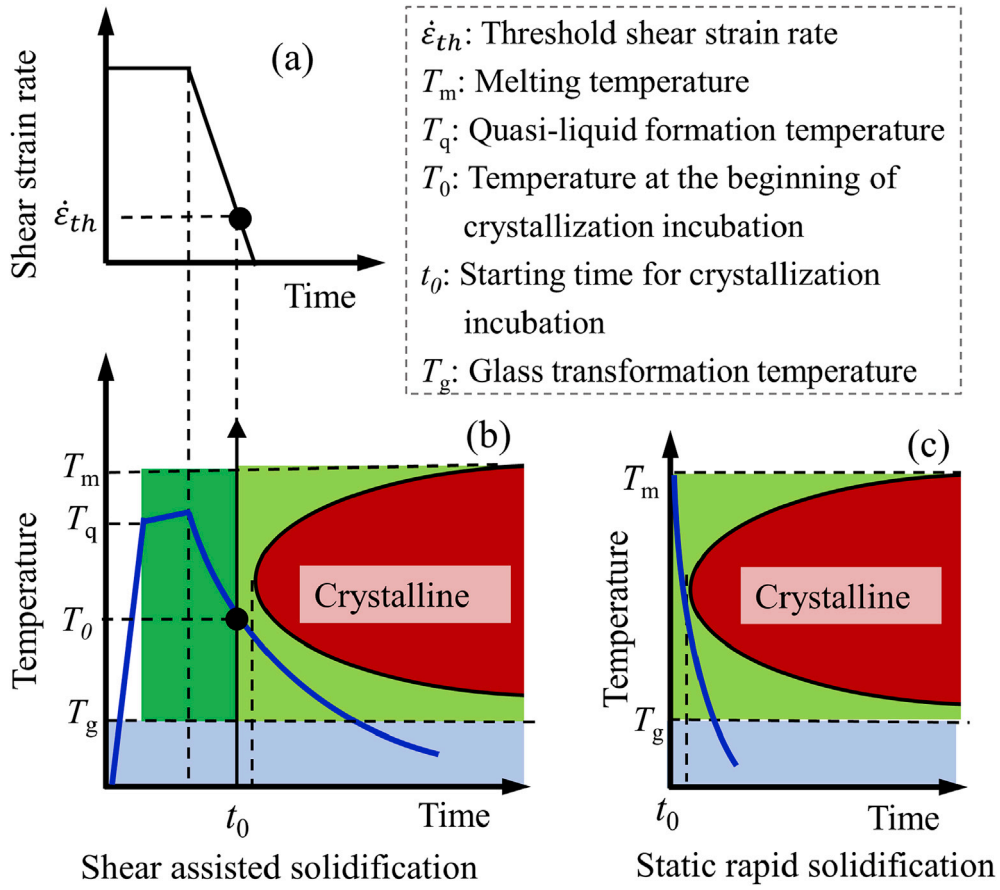

Fig. 10. Effect of nanoscale shear localization on the liquid-solid phase transformation. (a) Deformation history of the quasi-liquid alloy at the Al-Fe interface. (b) Dynamic time-temperature-transformation (TTT) diagrams of the quasi-liquid alloy at the Al-Fe interface under the effect of high-speed shear. (c) Static TTT diagram of a liquid alloy with the same chemical composition as the quasi-liquid alloy at the Al-Fe interface.

at the Al-Fe interface. Further study of the free energy of the various phases and the kinetics of diffusion are needed to elucidate this phenomenon.

Discussion

Based on the MD simulation and experimental results, we deduce a new nanoscale amorphization mechanism that can inhibit crystallization at the Al-Fe interface, which is schematically illustrated in Fig. 10. Interfacial sliding at a sufficiently high velocity (for continuum mechanics based shear localization modeling results, refer to a study by Pei and Dong [24,25]) and elevated temperature triggers interfacial premelting, leading to the formation of a nanoscale quasi-liquid layer. As a result, the applied shear deformation becomes confined within such a nanoscale quasi-liquid layer within which shear strain rates can reach the order of about 10^8 s^{-1}. This is referred to as nanoscale shear localization in this article. With such a high shear strain rate, atoms within the quasi-liquid layer are unable to organize themselves into an ordered crystalline structure. The presence of quasi-liquid at the Al-Fe interface allows diffusion of solute atoms from surrounding alloys into the quasi-liquid layer, forming a layer of quasi-liquid amorphous alloy. The quasi-liquid amorphous alloy can be maintained below the melting point as long as a sufficiently high shear strain rate is sustained.

From this condition, any decrease in the shear strain rate will lead to a temperature reduction within the quasi-liquid layer. At a given interface temperature, there exists a threshold shear strain rate ($\dot{\varepsilon}_{th}$), below which the cooling rate controls the onset of crystallization. The required $\dot{\varepsilon}_{th}$ is dependent on temperature and glass-forming alloy composition. If the temperature of the quasi-liquid amorphous alloy is already situated below the crystallization nose of the T-T-T diagram when the $\dot{\varepsilon}_{th}$ is reached, the amorphous state can be sustained under a relatively low cooling rate (Fig. 10b). In contrast, a much faster cooling rate is necessary for the same alloy to avoid the crystallization nose without an applied high shear strain rate, that is, under conventional rapid solidification conditions (Fig. 10c).

Interfacial premelting is the precursors of nanoscale shear localization under interfacial sliding conditions. Various factors can affect the occurrence of interfacial premelting, including alloying, interfacial sliding, and microstructure evolution. The premelting temperature can be reduced by adding an appropriate amount of solutes to Al alloys [26], which is likely to be an accompanying phenomenon of low eutectic temperature. The present study for the first time demonstrates that interfacial premelting can be promoted directly by interfacial sliding between Al and Fe crystals. Friction between bulk Al and Fe can also cause grain refinement in Al alloy through thermomechanical deformation and recrystallization. The thin 'amorphous' grain boundaries transferred to liquid-like state at elevated temperatures [27,28], promoting grain boundary sliding and grain rotation when the grains are fine enough [28–31]. Such grain

microstructure evolution is expected to promote the formation of premelting at the Al-Fe interface, but this is left for future work.

Conclusions

Sufficiently high interfacial sliding between an aluminum alloy and steel can generate a nanoscale quasi-liquid layer at their interface below the melting point of aluminum alloy, leading to a nanoscale shear localization confined within the quasi-liquid layer. The shear strain rate is equally distributed within the quasi-liquid layer. Because the thickness of the quasi-liquid layer is only several nanometers, the average shear strain rate can be higher than 10^8 s^{-1}, which is high enough to suppress the crystal nucleation within the quasi-liquid layer. The presence of a quasi-liquid layer at the Al-Fe interface allows diffusion of solute atoms from surrounding alloys into the quasi-liquid layer, forming a layer of quasi-liquid amorphous alloy. As long as a sufficiently high shear strain rate can be sustained until the interfacial temperature becomes lower than the crystallization nose of the alloy in the TTT diagram, a stable amorphous state at the interface can be retained at room temperature without relying on rapid solidification. This newly found interfacial amorphization mechanism, in addition to detailed mechanistic elucidation through our MD modeling results, has also been confirmed through our controlled experiments on the Al/Fe bimetallic system in this study.

Data availability

The data sets generated and/or analyzed in the present study are available from the corresponding author on reasonable request.

Author contributions

PD and WL designed the overall investigative approach, initiated and oversaw this study. AT reviewed intermediate MD and experimental results and provided guidance on alloy amorphization aspects of the study. FL and PD designed the experiments and FL implemented the experiments. FL and WK performed microstructure characterization. JZ and WL carried out MD modeling. FL designed some of the specific modeling cases and drafted the manuscript. All contributed to the result analysis and final preparation of the manuscript.

Declaration of Competing Interest

The authors declare the following financial interests/personal relationships which may be considered as potential competing interests: Fengchao Liu, Pingsha Dong, Wei Lu, and Alan Taub have filed a patent application (US Prov. App. 62956368).

Acknowledgements

This work was supported by University of Michigan College of Engineering startup grant, and FL and PD acknowledge the technical support from the Michigan Center for Materials Characterization - $(MC)^2$.

References

[1] A. Taub, E. De Moor, A. Luo, D.K. Matlock, J.G. Speer, U. Vaidya, Materials for automotive lightweighting, Annu. Rev. Mater. Res. 49 (2019) 327–359, https://doi.org/10.1146/annurev-matsci-070218-010134.

[2] K. Martinsen, S.J. Hu, B.E. Carlson, Joining of dissimilar materials, CIRP Ann. Manuf. Technol. 64 (2) (2015) 679–699, https://doi.org/10.1016/j.cirp.2015.05.006.

[3] N. Chen, H.-P. Wang, B.E. Carlson, D.R. Sigler, M. Wang, Fracture mechanisms of Al/steel resistance spot welds in coach peel and cross tension testing, J. Mater. Process. Technol. 252 (2018) 348–361, https://doi.org/10.1016/j.jmatprotec.2017.09.035.

[4] H. Springer, A. Kostka, E. Payton, D. Raabe, A. Kaysser-Pyzalla, G. Eggeler, On the formation and growth of intermetallic phases during interdiffusion between low-carbon steel and aluminum alloys, Acta Mater. 59 (4) (2011) 1586–1600, https://doi.org/10.1016/j.actamat.2010.11.023.

[5] I. Bataev, D. Lazurenko, S. Tanaka, K. Hokamoto, A. Bataev, Y. Guo, A. Jorge Jr., High cooling rates and metastable phases at the interfaces of explosively welded materials, Acta Mater. 135 (2017) 277–289, https://doi.org/10.1016/j.actamat.2017.06.038.

[6] Y. Sun, H. Fujii, N. Takaki, Y. Okitsu, Microstructure and mechanical properties of dissimilar Al alloy/steel joints prepared by a flat spot friction stir welding technique, Mater. Des. 47 (2013) 350–357, https://doi.org/10.1016/j.matdes.2012.12.007.

[7] J. Li, Q. Yu, Z. Zhang, W. Xu, X. Sun, Formation mechanism for the nanoscale amorphous interface in pulse-welded Al/Fe bimetallic systems, Appl. Phys. Lett. 108 (20) (2016) 201606, https://doi.org/10.1063/1.4947465.

[8] Z. Fan, H. Yu, C. Li, Interface and grain-boundary amorphization in the Al/Fe bimetallic system during pulsed-magnetic-driven impact, Scripta Mater. 110 (2016) 14–18, https://doi.org/10.1016/j.scriptamat.2015.07.035.

[9] M. Chen, J.W. McCauley, K.J. Hemker, Shock-induced localized amorphization in boron carbide, Science 299 (5612) (2003) 1563–1566, https://doi.org/10.1126/science.1080819.

[10] H. Ikeda, Y. Qi, T. Cagin, K. Samwer, W.L. Johnson, W.A. Goddard III, Strain rate induced amorphization in metallic nanowires, Phys. Rev. Lett. 82 (14) (1999) 2900, https://doi.org/10.1103/PhysRevLett.82.2900.

[11] S. Fukumoto, H. Tsubakino, K. Okita, M. Aritoshi, T. Tomita, Amorphization by friction welding between 5052 aluminum alloy and 304 stainless steel, Scripta Mater. 42 (8) (2000), https://doi.org/10.1016/S1359-6462(00)00299-2.

[12] R.B. Schwarz, C.C. Koch, Formation of amorphous alloys by the mechanical alloying of crystalline powders of pure metals and powders of intermetallics, Appl. Phys. Lett. 49 (3) (1986) 146–148, https://doi.org/10.1063/1.97206.

[13] F.C. Liu, P. Dong, W. Lu, A. Taub, Methods of joining dissimilar metals without detrimental intermetallics, US Prov. App (2019), 62956368.

[14] B. Slater, A. Michaelides, Surface premelting of water ice, Nature Rev. Chem. (2019) 1, https://doi.org/10.1038/s41570-019-0080-8.

[15] B. Li, F. Wang, D. Zhou, Y. Peng, R. Ni, Y. Han, Modes of surface premelting in colloidal crystals composed of attractive particles, Nature 531 (7595) (2016) 485, https://doi.org/10.1038/nature16987.

[16] Y. Li, L. Zang, D.L. Jacobs, J. Zhao, X. Yue, C. Wang, In situ study on atomic mechanism of melting and freezing of single bismuth nanoparticles, Nat. Commun. 8 (1) (2017) 1–8, https://doi.org/10.1038/ncomms14462.

[17] D.T. Limmer, Closer look at the surface of ice, Proc. Natl. Acad. Sci. Unit. States Am. 113 (44) (2016) 12347–12349, https://doi.org/10.1073/pnas.1615272113.

[18] E. Ma, Amorphization in mechanically driven material systems, Scripta Mater. 49 (10) (2003) 941–946, https://doi.org/10.1016/S1359-6462(03)00477-9.

[19] K.-i. Hirano, R. Agarwala, M. Cohen, Diffusion of iron, nickel and cobalt in aluminum, Acta Metall. 10 (9) (1962) 857–863, https://doi.org/10.1016/0001-6160(62)90100-1.

[20] G. Hood, The diffusion of iron in aluminium, Phil. Mag.: A J. Theor. Exper. Appl. Phys. 21 (170) (1970) 305–328.

[21] R. Suzuki, Y. Komatsu, K. Kobayashi, P. Shingu, Formation and crystallization of Al-Fe-Si amorphous alloys, J. Mater. Sci. 18 (4) (1983) 1195–1201, https://doi.org/10.1007/BF00551989.

[22] F.C. Liu, Z.Y. Ma, Influence of tool dimension and welding parameters on microstructure and mechanical properties of friction-stir-welded 6061-T651 aluminum alloy, Metall. Mater. Trans. 39a (10) (2008) 2378–2388, https://doi.org/10.1007/s11661-008-9586-2.

[23] P. Dong, F.W. Brust, Welding residual stresses and effects on fracture in pressure vessel and piping components: a millennium review and beyond, J Press Vess-T Asme 122 (3) (2000) 329–338, https://doi.org/10.1115/1.556189.

[24] X. Pei, P. Dong, A selectively-coupled shear localization model for friction stir welding process window estimation, Int. J. Mach. Tool Manufact. 123 (2017) 89–104, https://doi.org/10.1016/j.ijmachtools.2017.08.003.

[25] X. Pei, P. Dong, An improved friction stir shear localization model and applications in understanding weld formation process in alloy Ti-6-4, Int. J. Adv. Manuf. Technol. 95 (9–12) (2018) 3549–3562, https://doi.org/10.1007/s00170-017-1467-7.

[26] Y. Mishin, W. Boettinger, J. Warren, G. McFadden, Thermodynamics of grain boundary premelting in alloys. I. Phase-field modeling, Acta Mater. 57 (13) (2009) 3771–3785, https://doi.org/10.1016/j.actamat.2009.04.037.

[27] D. Guo, S. Song, R. Luo, W.A. Goddard III, M. Chen, K.M. Reddy, Q. An, Grain boundary sliding and amorphization are responsible for the reverse Hall-Petch relation in superhard nanocrystalline boron carbide, Phys. Rev. Lett. 121 (14) (2018) 145504, https://doi.org/10.1103/PhysRevLett.121.145504.

[28] H. Zhang, D.J. Srolovitz, J.F. Douglas, J.A. Warren, Grain boundariesexhibit the dynamics of glass-forming liquids, Proc. Natl. Acad. Sci. Unit. States Am. 106 (19) (2009) 7735–7740, https://doi.org/10.1073/pnas.0900227106.
[29] Z.Y. Ma, F.C. Liu, R.S. Mishra, Superplastic deformation mechanism of an ultrafine-grained aluminum alloy produced by friction stir processing, Acta Mater. 58 (14) (2010) 4693–4704, https://doi.org/10.1016/j.actamat.2010.05.003.
[30] P. Williams, Y. Mishin, Thermodynamics of grain boundary premelting in alloys. II. Atomistic simulation, Acta Mater. 57 (13) (2009) 3786–3794, https://doi.org/10.1016/j.actamat.2009.04.037.
[31] C. Gourlay, A. Dahle, Dilatant shear bands in solidifying metals, Nature 445 (7123) (2007) 70–73, https://doi.org/10.1038/nature05426.